Colin D. Flint and Anthony P. Matthews

Contribution from the Department of Chemistry, Birkbeck College, University of London WC1E 7HX, United Kingdom

Luminescence, Electronic Absorption, Infrared, and Raman Spectra of the *trans*-$Cr(py)_4F_2^+$ Ion

COLIN D. FLINT*[1] and ANTHONY P. MATTHEWS

Received September 16, 1974 AIC40650Q

The 80 and 5 K single-crystal absorption and luminescence spectra, 300 and 100 K diffuse-reflectance spectra, 300 and 80 K infrared spectra, and 300 K Raman spectra of *trans*-$[Cr(py)_4F_2]NO_3$ have been measured. The luminescence is caused by the $^2E_g(D_{4h}) \rightarrow {}^4B_{1g}$ transition and shows an electronic origin and about 30 vibronic origins. For most of these vibronic origins the vibrational motions can be specified. Progressions of up to 3 quanta of the symmetric Cr–F stretching mode are observed based on these origins. Four spin-allowed transitions are assigned from the reflectance spectra and their energies used to derive approximate values of the crystal field parameters. Six spin-forbidden transitions are also observed in the absorption spectra and each shows extensive vibronic structure which can be almost completely analyzed. The vibrational frequencies in these doublet states are compared with the ground-state frequencies. The differences in these frequencies and the intensity mechanisms of the vibronic origins and progressions are discussed using crystal field and MO models. There is strong evidence for chromium to pyridine π bonding in the ground state and in the low-lying doublet states.

Introduction

The $^4A_{2g} \rightarrow {}^2E_g$, $^2T_{1g}$, $^2T_{2g}(t_{2g}^3)$ transitions of octahedral chromium(III) complexes are of particular interest since, when they are not obscured by the stronger spin-allowed transitions, they usually show considerable vibronic structure. The analysis of this structure provides a source of data on vibronic effects in coordination complexes and on the relative chromium–ligand equilibrium distances in the initial and terminal states. This well-resolved structure is a consequence of both the initial and terminal states being derived almost exclusively from the t_{2g}^3 configuration. The potential surfaces of the states therefore have the same shape and lie almost directly above each other on a configuration coordinate diagram. Where there are significant differences in the positions and/or shapes of the potential surfaces, these can be attributed either to the mixing of configurations *via* spin–orbit coupling[2,3] or to the sensitivity of the electron–electron repulsion integrals to the metal–ligand distance.[4] Configuration interaction *via* the coulombic operator is usually too small to have observable effects on the vibronic structure.

A tetragonal component of the crystal field removes the degeneracy of the t_{2g} orbitals. The $^4A_{2g}$, ^2E_g, $^2T_{1g}$, and $^2T_{2g}(O_h)$ states are not split in the first order and the $^4A_{2g}$ and $^2E_g(O_h)$ states are not split in the second order. However interaction between the $^2E_g(D_{4h})$ components of the $^2T_{1g}(O_h)$ and $^2T_{2g}(O_h)$ states under the tetragonal perturbation ($\langle {}^2E_g, {}^2T_{1g}|V_{tet}|{}^2E_g, {}^2T_{2g}\rangle = 3Ds - 5Dt$) may become appreciable compared with the zeroth-order separation of these states. This interaction affects the electronic spectra of tetragonal chromium(III) complexes in two important ways.

(i) There is a large second-order splitting of the $^2T_{1g}$ and $^2T_{2g}$ states. The energy of the lower $^2E_g(D_{4h})$ state is depressed by about $(3Ds - 5Dt)^2/(6B + 2C)$ and one of its spin–orbit components becomes the lowest excited energy level when $|3Ds - 5Dt| > ca.$ 2000 cm^{-1}. The energy of the higher ^2E_g states[5] will be raised but by less than $(3Ds - 5Dt)^2/(6B + 2C)$ because this state is repelled by other ^2E_g states which lie further to high energy.

(ii) The ^2E_g ($Ds = Dt = 0$) wave functions are mixed[6] to give the new tetragonal wave functions. For brevity we refer to the lower energy of these as a^2E_g and the higher energy as b^2E_g. If $3Ds - 5Dt$ is positive,[7] this mixing results in the a^2E_g state having an increased contribution from the $(xy)^2(xz)$ or $(xy)^2(yz)$ configurations[6] and hence metal electron density is transferred from around the z axis[8] into the xy plane in this state. There will be a corresponding transfer of electron density in the opposite direction in the b^2E_g state. The directions of the transfers are reversed for negative $(3Ds - 5Dt)$. These changes in the distribution of metal d-electron density from the spherically symmetric distribution in cubic Cr(III) complexes are exactly as expected from a simple MO viewpoint. A positive $(3Ds - 5Dt)$ corresponds to the ligands on the z axis being stronger π donors than the ligands on the x and y axes (the McClure[8] parameter $\delta\pi = 3Ds - 5Dt$). This π-donor effect raises the energy of the (xz) and (yz) orbitals relative to the xy orbital. The energy of the a^2E_g state is then minimized by increasing the contribution to this state from the $(xy)^2(xz)$ or $(xy)^2(yz)$ configurations as previously. These considerations suggest that for a complex with a strong π donor (Z) on the z axis and ligands (X) without π orbitals suitable for bonding on the x and y axes, the Cr–Z bond distance will be shorter and the bond strength greater in the a^2E_g state than in the $^4B_{1g}$ ground state. Although the Cr–X distance will not be influenced by π bonding, shortening the Cr–Z bond length will result in an increase in the Cr–X distance in the a^2E_g state because the effective charge on the chromium will be reduced. The differences in bond lengths between the $^4B_{1g}$ and b^2E_g states will be in the opposite direction. The changes in equilibrium metal–ligand distances between the $^4B_{1g}$ and ^2E_g states will give appreciable intensity to progressions in the totally symmetric Cr–Z and Cr–X modes based on the electronic and vibronic origins of the $^4B_{1g} \leftrightarrow a^2E_g$ and $^4B_{1g} \rightarrow b^2E_g$ transitions. The differences in bond strengths would be expected to result in appreciably different metal–ligand stretching frequencies in the initial and terminal states.

The lowering of the energy of the a^2E state and the progressions in the $a^2E_g \rightarrow {}^4B_{1g}$ luminescence of *trans*-$Cr(en)_2F_2^+$ (en = 1,2-diaminoethane) have been observed[6] but the other consequences of interaction between ^2E_g, $^2T_{1g}$ and ^2E_g, $^2T_{2g}$ states have not been detected because of experimental difficulties. In this paper we report a detailed study of the electronic and vibrational spectra of *trans*-$[Cr(py)_4F_2]NO_3$ (py = pyridine). For this compound a number of factors are favorable for a rather thorough examination of these consequences. First, the magnitude of $3Ds - 5Dt$ is even larger than in *trans*-$Cr(en)_2F_2^+$, which increases the magnitude of the effects. Second, the values of the crystal field parameters are such that the $^4B_{1g} \rightarrow a^2E_g$, $^2B_{1g}$, $^2A_{1g}$, $^2A_{2g}$, b^2E_g transitions occur in regions where they are not obscured by the spin-allowed transitions. Third, the vibrational and vibronic spectra are very well resolved. Fourth, the vibrational properties of the pyridine ligand, although complex, are well understood. Fifth, large crystals of the salt are easily grown from the nonsolvolytic solvent chloroform. There are no X-ray

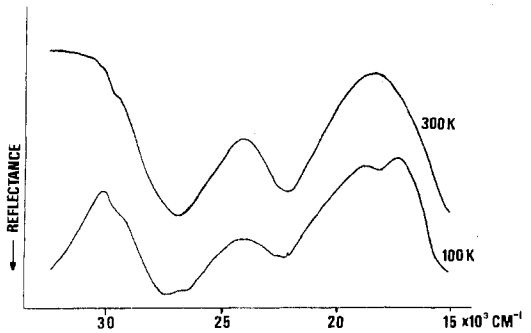

Figure 1. Diffuse-reflectance spectra of *trans*-$[Cr(py)_4F_2]NO_3$.

structural data available for this salt but all our results are consistent with the CrN_4F_2 entity having an *almost* perfect D_{4h} stereochemistry.

Experimental Section

Materials. *trans*-$[Cr(py)_4F_2]NO_3$ and *trans*-$[Cr(py)_4F_2](ClO_4)$ were prepared by the method of Glerup, *et al.*[10] Several large crystals of the nitrate salt were grown by the slow evaporation of a chloroform solution at room temperature in the dark. These crystals were polished down to convenient thicknesses for the measurement of the weak spin-forbidden bands in absorption. This thickness was less than 1 mm for the $^4B_{1g} \rightarrow b^2E_g$ transition and greater than 3 mm for the $^4B_{1g} \rightarrow a^2E_g$ transition. Great difficulty was experienced in obtaining crystals that were sufficiently thin for the measurement of the absorption spectra near the spin-allowed transitions. When apparently suitable crystals were obtained, the absorption spectra were not strongly polarized. Since the main purpose of this work was to study the spin-forbidden transitions, the approximate positions of the quartet states were obtained from the 100 K diffuse-reflectance spectra. Fortunately the splittings of the octahedral quartet states were sufficiently large for the components to be located to within ±200 cm^{-1} by this technique. The spin-forbidden transitions were not strongly polarized. All measurements were carried out on at least two crystals of the nitrate grown from different preparations of the salt and gave identical results. In addition the infrared, electronic reflectance, luminescence, and $^4B_{1g} \rightarrow {}^2B_{1g}$, $^2A_{1g}$, $^2A_{2g}$ absorption spectra of the perchlorate salt were measured. The results were essentially identical, the main differences being the bands due to the anions in the infrared spectrum and small changes in the vibrational frequencies and the positions of the electronic origins.

Instruments. Luminescence spectra were measured using a Hilger-Engis D460 monochromator fitted with a 1200-line/mm grating blazed at 750 nm, a cooled 150CVP(S1) photomultiplier, and phase-sensitive detection. The excitation source was a modulated[11] HBO 200 mercury arc and a 1/4-m monochromator adjusted to pass the 546-nm line. Absorption spectra were measured using the D460 monochromator, cooled S1 or S20 photomultipliers, and a stabilized tungsten source. Spectral slit widths of *ca.* 3 cm^{-1} were used for both absorption and emission spectra and this did not limit the resolution achieved. The samples were mounted in an Oxford Instruments CF100 cryostat. Sample temperatures were measured using a CLTS device.

Infrared spectra were measured using a Perkin-Elmer 457 or Beckman RIIC FS720 interferometer *via* the PCMU service at Harwell, U.K.

Raman spectra were measured using a Cary 81 instrument with 6471-Å Kr^+ excitation and a spinning-pellet sample holder.

Diffuse-reflectance spectra were measured using a Unicam SP700 instrument fitted with an SP735 reflectance accessory and a low-temperature cell constructed in this laboratory.

Spin-Allowed Transitions

We were unable to obtain single-crystal polarized absorption spectra of either the nitrate or perchlorate salts in the region of the spin-allowed transitions. The 300 and 100 K diffuse reflectance electronic spectra of the nitrate salt are shown in Figure 1. The reflectance spectra of the perchlorate salt were identical. In the crystal field limit *Ds* and *Dt* for a D_{4h} MX_4Z_2 chromophore may be written

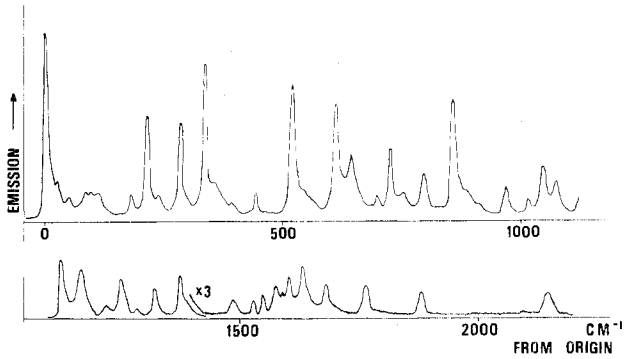

Figure 2. The 546-nm excited luminescence spectrum of a single crystal of *trans*-$[Cr(py)_4F_2]NO_3$ at 5 K. The electronic origin is at 13,902 cm^{-1}.

$$Ds = Cp(Z) - Cp(X)$$

$$Dt = {}^4/_7[Dq(Z) - Dq(X)]$$

where *Cp* is the second-order radial parameter defined by Gerloch and Slade[7] and the sign convention of Liehr[7] is used. These relationships, the spectrochemical series, and trends in the values of *Cp*[7] suggest that both *Ds* and *Dt* will be greater in *trans*-$Cr(py)_4F_2^+$ than in *trans*-$Cr(en)_2F_2^+$,[6,12] although *Dt* will probably still be just negative. The splitting of the $^4T_{2g}$ state by the tetragonal field depends mainly on *Dt* whereas the splitting of the lower $^4T_{1g}$ state depends mainly on *Ds*. We expect therefore that the $^4T_{2g}$ splitting will be less in the pyridine compound than in the ethylenediamine complex with the ^4E_g state still at lowest energy and that the splitting of the lower $^4T_{1g}$ state will be greater in the pyridine compound. Examination of the spectra then strongly suggests that the bands at 17,000, 18,500, 24,300, and 29,900 cm^{-1} (each ±200 cm^{-1}) are assigned as transitions from the $^4B_{1g}$ ground state to the ^4E_g ($^4T_{2g}$, O_h), $^4B_{2g}$, ^4E_g ($^4T_{1g}$, O_h), and $^4A_{2g}$ states, respectively. The energy of the $^4B_{2g}$ state [which depends only $Dq(py)$] is appreciably lower than in the ethylenediamine compound as expected. Alternative assignments cannot be reconciled with reasonable values of the crystal field parameters. These assignments are supported by crystal field calculations involving the doublet and quartet states (see below) and by the observed strong temperature dependence of the intensity of the $^4B_{1g} \rightarrow {}^4B_{2g}$ transition and the much smaller temperature dependence of the intensity of both $^4B_{1g} \rightarrow {}^4E_g$ transitions. This behavior parallels that of the ethylenediamine compound[12] and the frequencies and activities of the enabling vibrations are expected to be similar in the two cases.

Spin-Forbidden Transitions

Luminescence and Vibrational Spectra. The 546-nm excited 5 K luminescence spectrum of a single crystal of *trans*-$[Cr(py)_4F_2]NO_3$ is shown in Figure 2. For values of the crystal field parameters consistent with the positions of the quartet states the lowest excited state is the ^2E_g and the emission is assigned as being due to the transition from the lower spin–orbit component of this state to the $^4B_{1g}$ ground state. The expected small splitting (*ca.* 0.5 cm^{-1}) of the ground state[13] was not resolved in any of our measurements. This assignment is confirmed by the vibronic analysis of the luminescence and absorption spectra and by crystal field calculations (see below). The electronic origin is easily identified as the strong band at highest energy. This identification is supported by the 5 K electronic absorption spectrum and by the location of a large number of vibronic origins based on this electronic origin involving vibrational intervals similar to those observed in the room-temperature and 80 K infrared spectra (Table I).

The N–Cr–N bending, Cr–py torsion, and Cr–py rocking

Table I. Vibrational Intervals[a] in the 5 K $^2E_g \rightarrow {}^4B_{1g}$ (D_{4h}) Luminescence Spectrum and the Infrared[b] and Raman Spectra of *trans*-$[Cr(py)_4F_2]NO_3$ (cm^{-1})

Infrared[b]	Raman	Luminescence	Assignment
		27 w	N–Cr–N bends, Cr–py rocks, and torsions
		54 w	
		88 w	
100 w		102 w, br	
130 w		120 mw	
187 w		186 mw	
	204 m		α_{1g}(Cr–N) str
220 w		213 ms	α_{2u}- or β_{2u}(F–Cr–N) bend
247, 242 m		242 mw	ϵ_u(F–Cr–N) bend
283 m		284 ms	a_{2u}- or β_{2u}(F–Cr–N) bend
334, 326 s		340 s	ϵ_u(Cr–N) str
		366 w	
		394 w	
450, 444 s		450 m	Pyridine (16b)[c]
	520 m	521 s	α_{1g}(Cr–F) str
612 s		614 s	α_{2u}(Cr–F) str
657, 650, 645 s	653 m	650 ms	Pyridine (6a, 6b)
710, 700 s		703 mw	Pyridine (11)
		739 m	213 + 521
780, 768 s		770 w	Pyridine (4)
		802 m	284 + 521
831 m			NO_3^- (ν_2)
		860 ms	340 + 521
890, 884 m			Pyridine (5)
		972 mw	450 + 521
1016, 1012 s	1022 vs	1014 w	Pyridine (1)
1045 s	1045 s	1041 ms	Pyridine (12) and 2 × 521
1068 s		1073 m	Pyridine (18a)
		1126 s	614 + 521
1152 m			Pyridine (15)
		1169 ms	650 + 521
1213 ms		1217 mw	Pyridine (9a)
1242 mw	1231 m		Pyridine (3)
		1250 m	213 + 2 × 521
		1285 w	242 + 2 × 521
		1319 m	284 + 2 × 521
1340 m			Pyridine (6a + 10b)
1365 m			Pyridine (14)
		1375 ms	340 + 2 × 521
1480		1484 mw	Pyridine (19a) and 450 + 2 × 521
		1538 mw	1014 + 521
		1551 mw	3 × 521
	1572 m	1570 m	Pyridine (8b)
		1592 w	1073 + 521
1605 s	1610 m	1606 mw	Pyridine (8a)
		1637 ms	614 + 2 × 521
		1689 m	650 + 2 × 521
		1764 m	213 + 3 × 521
		1887 m	340 + 3 × 521
		2150 w	614 + 3 × 521

[a] The origin is at 11,902 cm^{-1}. [b] The bands below 400 cm^{-1} were measured at 80 K; those at higher energy, at room temperature. [c] The notation for the internal pyridine modes is that used by L. K. Wilmshurst and H. J. Bernstein, *Can. J. Chem.*, 35, 1183 (1957).

vibrational modes are expected to be of low energy and are probably responsible for the complex group of bands between 20 and 200 cm^{-1} from the electronic origin. Coupling of these modes with lattice vibrations may also produce spectral features in this region. The Cr–N stretching and F–Cr–N bending motions form bases for vibrational modes of symmetries α_{1g}, β_{1g}, ϵ_u and α_{2u}, β_{2u}, ϵ_g, ϵ_u, respectively, in D_{4h} symmetry.[6] Of these the four u modes can be vibronically active. There are four bands between 213 and 340 cm^{-1} from the origin which must involve mainly these motions. The two bands at 242 and 340 cm^{-1} are each just split into two components of comparable intensity in the infrared spectra of both the perchlorate and nitrate salts. These splittings are not due to nonequivalent sites in the crystal because no splittings of any of the electronic origins are observed in the absorption spectra. Correlation field splittings[14] also seem unlikely. It is probable that the splittings arise from a small distortion from D_{4h} symmetry relieving the degeneracy of (and hence identifying) the two ϵ_u modes. In the luminescence spectrum the 242- and 340-cm^{-1} bands have a half-height width of *ca.* 12 cm^{-1} which precludes the resolution of the splitting. Comparison of the infrared and luminescence spectra of $Cr(py)_4F_2^+$ with those of $Cr(py)_4Cl_2^+$, $Cr(py)_4Br_2^+$, and other compounds shows that the 340 cm^{-1} involves mainly ϵ_u(Cr–N) stretching and the 242-cm^{-1} band mainly ϵ_u(N–Cr–F) bending. The vibrational frequencies in the a^2E_g and b^2E_g states support these assignments. The only Raman band observed in this region is at 204 cm^{-1} and is assigned as the α_{1g}(Cr–N) stretching mode. The difference between this frequency and 213 cm^{-1} is significant.

The α_{1g}(Cr–F) stretching mode occurs at 520 cm^{-1} in the Raman spectrum. There is no absorption in this region in the infrared spectrum showing that the complex ion is essentially centrosymmetric but this interval appears strongly in the luminescence spectrum. The first two or three members of progressions in this mode appear based on the origin and all of the stronger vibronic origins (Table I). None of the bands assigned as progressions appear strongly in the infrared spectrum. The relative intensities of the members of the progressions are about 100:90:50:15 which correspond[15] to a shortening of the equilibrium Cr–F bond distance by about 0.1 Å in the a^2E_g state relative to the ground state through the mechanism outlined in the Introduction.

This change in bond length is greater than that observed in *trans*-$Cr(en)_2F_2^+$ as expected since $(3Ds - 5Dt)/(6B + 2C)$ is larger in the pyridine compound. The members of these progressions show perceptible shifts owing to anharmonicity. The assignment of the 520-cm^{-1} band is confirmed by the vibrational frequencies in the a^2E_g and b^2E_g states and by the absence of this band in the $^4B_{1g} \rightarrow {}^2B_{1g}$, $^2A_{2g}$, $^2A_{2g}$ absorption spectra. The corresponding vibrational mode in *trans*-$Cr(en)_2F_2^+$ occurs[6] at 512 cm^{-1}. The α_{2u}(Cr–F) stretching mode appears strongly at 614 cm^{-1} in the infrared and luminescence spectrum. Again this assignment is supported by the vibrational frequencies in the a^2E_g and b^2E_g states.

Analogy with the luminescence spectrum of *trans*-$Cr(en)_2F_2^+$ would suggest that the shortening of the Cr–F bond length in the a^2E state will be accompanied by a lengthening of the Cr–N bond length and hence the appearance of progressions in the 204-cm^{-1} α_{1g}(Cr–N) stretching mode in the luminescence spectrum. These progressions have not been observed and it is possible to put an upper limit of 0.01 Å on the difference between the Cr–N bond lengths in the initial and terminal states. We attribute this difference in behavior of the two compounds to enhanced metal to pyridine π bonding in the a^2E_g state relative to the ground state (see Discussion).

There remain a number of bands in the luminescence spectrum which are coincident with bands in the infrared spectrum. They can only be assigned as internal modes of the pyridine ring. Many of these bands are split into two components separated by a few wave numbers in the infrared spectrum and also occur in the Raman spectrum. This is exactly as expected for internal pyridine modes since each vibrational mode of the isolated pyridine molecule gives two u and two g vibrational modes in a centosymmetric complex. Coupling between these modes and the small departure from D_{4h} symmetry will remove any degeneracies. The intensity of these vibronic origins indicates that there is appreciable interaction between the pyridine π system and the chromium t_{2g} orbitals.

Absorption Spectra. The 5 K single-crystal absorption spectrum of the nitrate salt in the region of the $^4B_{1g} \rightarrow a^2E_g$ transition is extremely weak. The features that were con-

Table II. $^4B_{1g} \rightarrow a^2E_g(D_{4h})$ Absorption Spectrum of *trans*-$[Cr(py)_4F_2]NO_3$ at 5 K

Band position,[a] cm^{-1}	Assignment[b]
11902 s	$0 \rightarrow 0'$
11959 m	$0' + 57$
11989 m	$0' + 87$
12109 m	$0' + 213$
12183 s	$0' + 281$
12218 s	$0 \rightarrow 0''$
12252 s	$0' + 351$
12428 w	$0'' + 213$
12458 s	$0' + 556$
12504 s	$0'' + 286$
12542 s	$0' + 640$
12570 m	$0'' + 352$
12667 s	$0' + 213 + 556$
12737 m	$0' + 281 + 556$
12781 m	$0'' + 563$
12801 s	$0' + 351 + 556$
12859 m	$0'' + 641$
13009 m	$0' + 2 \times 556$
13095 s	$0' + 640 + 556$
13120 m	$0'' + 352 + 563$?
13354 w	$0' + 351 + 2 \times 556$

[a] Intensities are relative; the strongest features are of comparable optical density to the weakest reported features in the $^4B_{1g} \rightarrow {}^2B_{2g}$, $^2A_{1g}$, $^2A_{2g}$ spectrum. [b] The two spin-orbit components of the ^2E_g state are designated 0' and 0''. Assignments of the vibrational modes are given in Table IV.

sistently observed in several scans of each of several crystals are given in Table II. The a^2E_g state is expected to be split into two components separated by a few hundred wave numbers by spin–orbit coupling. The lower of the expected pair of electronic origins is coincident with the origin observed in the luminescence spectrum. The second origin is probably a band 316 cm^{-1} to high energy of this origin which has no counterpart in the luminescence spectrum. It is then possible to assign almost all of the remaining bands as vibronic origins involving vibrations of the CrN_4F_2 entity analogous to those observed in the luminescence spectrum on these two electronic origins and as progressions in the α_{1g}(Cr–F) stretching mode based on the electronic and vibronic origins. As far as can be judged the relative intensity of the electronic and vibronic origins and the progressions is similar to that observed in the luminescence spectrum.

The α_{1g}- and α_{2u}(Cr–F) stretching modes are both *ca.* 35 cm^{-1} higher in frequency in the a^2E_g state than in the ground state and the ϵ_u(Cr–N) bending mode is about 10 cm^{-1} higher than in the ground state. The α_{2u}- and β_{2u}(N–Cr–F) bending modes have essentially the same frequency in the two states.

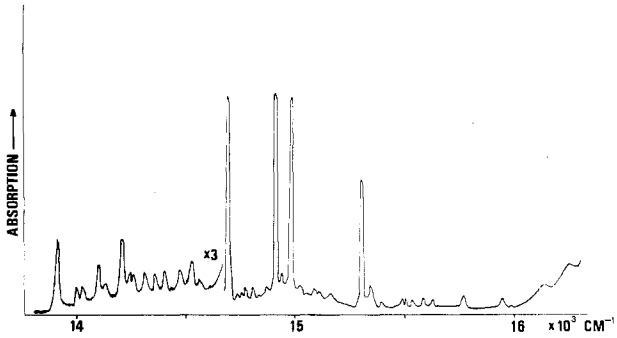

Figure 3. Single-crystal 5 K electronic absorption spectrum of *trans*-$[Cr(py)_4F_2]NO_3$ in the region of the $^2B_{1g} \rightarrow {}^2A_{1g}$, $^2A_{2g}$ transitions.

This is very much as expected from the crystal field and MO arguments presented in the Introduction and the interpretation of the luminescence spectrum. These changes also serve to confirm the assignments of the skeletal vibrations.

To high energy of the $^4B_{1g} \rightarrow {}^2E_g$ transitions there is a complex group of stronger lines (Figure 3). Three electronic transitions, $^4B_{1g} \rightarrow {}^2B_{1g}$, $^2A_{1g}$, and $^2A_{2g}$, are expected in this region each consisting of an electronic origin and associated vibronic origins. The medium strength band at lowest energy in this group is assigned as one of these electronic origins because many of the features in the region 14,000–14,600 cm^{-1} can be assigned as vibronic origins involving vibrational intervals similar to those giving the strongest vibronic origins in the $^2E_g \rightarrow {}^4B_{1g}$ transition (Table III). Similarly the strong band at 14,677 cm^{-1} is assigned as another electronic origin since it is then possible to assign more than ten bands in the region 14,700–16,250 cm^{-1} as vibronic origins on this origin. This is supported by the 80 K absorption spectrum in which the vibronic origins involving vibrational frequencies of less than 230 cm^{-1} can be observed with the expected intensities in the hot-band absorption spectrum. The identification of the third electronic origin is more difficult. If any of the otherwise unassigned bands are attributed to the third origin, then it is not possible to locate any of the expected vibronic origins. However if the prominent band at 14,188 cm^{-1} which is in the expected position for a vibronic origin on the lowest electronic origin is also due to an electronic origin, then a number of the expected vibronic origins on this 14,188-cm^{-1}

Table III. $^4B_{1g}$, $^2B_{1g}$, $^2A_{1g}$, $^2A_{2g}(D_{4h})$ Absorption Spectrum of *trans*-$[Cr(py)_4F_2]NO_3$ at 5 K

Band position, cm^{-1}	Assignment[a]	Band position, cm^{-1}	Assignment[a]
13,914 m	$^4B_{1g}$ $^2B_{1g}$	14,902 s	$^4B_{1g}$ $^2A_{1g} + 703$, $^2A_{2g} + 213$
14,011 vw	$^2B_{1g} + 97$	14,932 m	$^2B_{1g} + 1018$, $^2A_{2g} + 243$
14,035 vw	$^2B_{1g} + 121$	14,972 s	$^2A_{2g} + 284$
14,100 mw	$^2B_{1g} + 186$	15,022 w	$^2A_{2g} + 333$
14,130 w	$^2B_{1g} + 216$	15,089 w	$^2A_{1g} + 889$
14,200 m	$^2B_{1g} + 286$, $^2A_{1g}$	15,158 w	
14,241 vw		15,297 ms	$^2A_{2g} + 608$
14,261 vw	$^2B_{1g} + 347$	15,348 w	$^2A_{2g} + 659$
14,366 w	$^2B_{1g} + 452$	15,488 w	$^2B_{1g} + 1570$
14,407 w	$^2A_{1g} + 207$	15,507 w	$^2A_{1g} + 1307$
14,478 w	$^2A_{1g} + 278$	15,544 w	$^2A_{1g} + 1344$
14,530 m	$^2B_{1g} + 616$, $^2A_{1g} + 330$	15,580 w	$^2A_{1g} + 1380$
14,608 w	$^2B_{1g} + 703$	15,626 w	
14,689 s	$^2A_{2g}$	15,764 w	$^2A_{1g} + 1575$, $^2A_{2g} + 1075$
14,721 w	$^2A_{2g} + 27$	15,935 m	$^2A_{2g} + 1253$
14,744 w	$^2A_{2g} + 55$	16,124 m	
14,781 w	$^2A_{2g} + 92$	16,249 m	$^2A_{2g} + 1570$
14,810 w	$^2A_{1g} + 610$, $^2A_{2g} + 121$		
14,878 w	$^2A_{2g} + 189$		

[a] The vibrational frequencies are very similar to those in the $^4B_{1g}$ states so that assignments of the vibrational modes may be obtained from Table I.

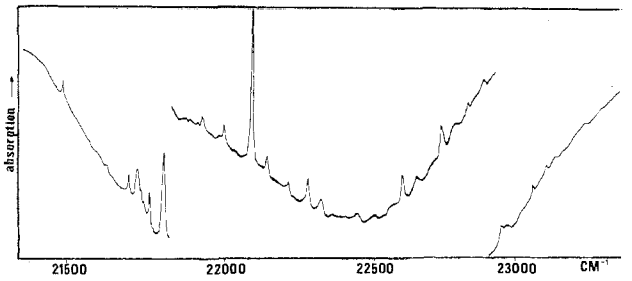

Figure 4. Single-crystal 5 K electronic absorption spectrum of *trans*-$[Cr(py)_4F_2]NO_3$ in the region of the $^4B_{1g} \rightarrow b^2E_g$ transition.

Table IV. Comparison of Vibrational Frequencies in the Ground State and Excited Doublet States[a]

Mode	$^4B_{1g}$	a^2E_g	$^2B_{1g}$	$^2A_{1g}$	$^2A_{2g}$	b^2E_g
α_{2u}- or β_{2u}- (F-Cr-N) bend	213	213	216	207	213	212
	284	284	(286)	278	284	278
ϵ_u(F-Cr-N) bend	242				243	(238)
ϵ_u(Cr-N) str	340	352	347	(330)	333	323
α_{1g}(Cr-F) str	521	558				512
α_{2u}(Cr-F) str	614	641	(616)	610	608	604

[a] Values in parentheses may be in error due to bands overlapping.

band can be located. The analysis is complicated by overlapping of transitions and by the changes in relative intensity of the vibronic origins in different transitions and is somewhat uncertain. A number of internal pyridine modes appear as relatively strong vibronic origins as in the luminescence spectra. Progressions in totally symmetric modes are not observed in any of the origins but they are not expected to have appreciable intensity since the d-electron distribution in the $^2B_{1g}$, $^2A_{1g}$, and $^2A_{2g}$ states is essentially the same as in the $^4B_{1g}$ ground state. For values of the crystal field parameters consistent with the positions of the quartet states, the doublet states are in order of increasing energy ^2E_g, $^2B_{1g}$, $^2A_{1g}$, and $^2A_{2g}$, as given in Tables II and III. The only unexplained feature of these assignments is the high intensity of the $^4B_{1g} \rightarrow {}^2A_{2g}$ transition relative to the other spin-forbidden transitions. We return to this problem in the next section.

Between the broad $^4B_{1g} \rightarrow {}^4B_{2g}$ and $^4B_{1g} \rightarrow {}^4E_g$ transitions a further group of sharp spin-forbidden bands was observed (Figure 4). Three transitions $^4B_{1g} \rightarrow {}^2B_{2g}$ and $^4B_{1g} \rightarrow \Gamma_6$, $\Gamma_7(b^2E_g)$ are expected to occur in this region. If the lowest energy band observed is assigned as an electronic origin, the spectrum has a close similarity to the $a^2E_g \rightarrow {}^4B_{1g}$ luminescence transition but with the intensity of the progressions rather lower. Almost all of the observed lines can be assigned as vibronic origins involving vibration intervals similar to but not identical with those observed in the luminescence spectrum and progressions in a mode of 512 cm^{-1} based on this origin (Tables IV and V). The 512-cm^{-1} interval is very much as expected for the α_{1g}(Cr-F) stretching mode in the b^2E_g or $^2B_{2g}$ states. Thus a satisfactory analysis of the observed spectrum can be made assuming only one of the expected transitions is involved. There is, however, at least one difficulty in this analysis. The band 238 cm^{-1} above the origin, although almost coincident with an expected vibronic origin, is relatively much stronger than the corresponding band in any of the other six spin-forbidden transitions and it has a shoulder on the high-energy side. More significantly, the first and second members of progressions in the 512-cm^{-1} mode based on the 238-cm^{-1} band are not observed although the progressions on the vibronic origins at 212 and 278 cm^{-1} are easily detected. We conclude that the 238-cm^{-1} band cannot be part of the transition responsible for most of the features but we are unable to give a definite assignment.

The assignment of the electronic transition responsible for most of this group of lines is not straightforward. The vibrational frequencies in the b^2E_g and $^2B_{2g}$ states are not expected to be sufficiently different to permit a clear distinction (see below) and a strong-field crystal field calculation cannot give the energies of the doublet states with sufficient accuracy although it would be expected to reproduce the correct ordering and separation of the b^2E_g and $^2B_{2g}$ states. Using values of the crystal field parameters derived from a least-squares fit to the observed band positions (see below) the b^2E_g state is predicted to lie *ca.* 1400 cm^{-1} above the $^2B_{2g}$ state. The energy of the $^2B_{2g}$ state is almost independent of the crystal field parameters but a strong function of the interelectronic repulsion parameters. The energy of the $^2B_{2g}$ state in *trans*-$Cr(py)_4F_2^+$ will then be significantly lower than the lowest component of the $^2T_{2g}(O_h)$ state in *trans*-$Cr(ox)_2(H_2O)_2$ and $Cr(ox)_3^{3-}$ (20,860[16] and 20,524 cm^{-1} [17]) because the $^2E_g(O_h)$ states in the pyridine compound are *ca.* 500 cm^{-1} lower in energy than the ^2E_g states in the oxalato complexes. This suggests that the $^2B_{2g}$ state in the pyridine compound should lie at *ca.* 20,000 cm^{-1} (where it will be obscured by the $^4B_{1g} \rightarrow {}^4B_{2g}$ transition) with the b^2E_g state between 21,000 and 22,000 cm^{-1}. We therefore tentatively assign the 21,487-cm^{-1} origin as one of the components of the $^4B_{1g} \rightarrow b^2E_g$ transition. The other component may be weakened and broadened by rapid relaxation to this component or to the $^4B_{2g}$ state so that only a few of its features (*e.g.*, the band at 238 cm^{-1} above the origin) are observable. The sharper lines between 22,550 and 23,250 cm^{-1} clearly show the effects of Sturge–Fano[18] antiresonance with $q \simeq -2$.

Table V. $^4B_{1g} \rightarrow b^2E_g$ Electronic Absorption Spectrum of *trans*-$[Cr(py)_4F_2]NO_3$ at 20 K

Band position, cm^{-1}	Assignment[a]
21,487 m	$0 \rightarrow 0'$
21,538 vw	$0' + 51$
21,570 vw	$0' + 83$
21,626 vw	$0' + 139$
21,699 m	$0' + 212$
21,725 ms	See text
21,739 sh	See text
21,810 s	$0' + 323$
21,929 m	$0' + 442$
21,999 m	$0' + 512$
22,091 vs	$0' + 604$
22,143 w	$0' + 656$
22,209 w	$0' + 212 + 512$
22,278 w	$0' + 278 + 512$
22,323 w	$0' + 323 + 512$
22,441 w	$0' + 442 + 512$
22,499 w	$0' + 1012$ or 2×512
22,557	$0' + 1070$
22,598 mw	$0' + 604 + 512$
22,649 br	$0' + 1162$ or $656 + 512$
22,731 m	$0' + 1244$
22,778 w	$0' + 278 + 2 \times 512$
22,824 w	$0' + 323 + 2 \times 512$
22,882 w	
22,942 w	$0' + 442 + 2 \times 512$
22,962 w	$0' + 1475$
23,053 w	$0' + 1566$
23,104 w	$0' + 604 + 2 \times 512$
23,130 vw	
23,157 vw	$0' + 656 + 2 \times 512$
23,238 vw	$0' + 212 + 3 \times 512$

[a] See footnote *b* of Table II.

Discussion

Crystal Field Calculations. To confirm the assignments of the transitions and the mechanism of the bond length changes we carried out least-squares fits to the observed energies of the four lowest quartets and the a^2E_g, $^2B_{1g}$, $^2A_{1g}$, and $^2A_{2g}$ states. The procedure was as described previously but the value of *Dq* was also allowed to vary. A typical set of results is shown in Table VI. The fit is very satisfactory considering the

Table VI. Crystal Field Parameters Obtained from a Least-Squares Fit to Observed Band Positions of *trans*-$[Cr(py)_4F_2]NO_3$

	Obsd ν, cm^{-1}	wt	Calcd ν,[a] cm^{-1}	Parameters,[a] cm^{-1}
a^2E_g	12,400[b]	1	12,430	
$^2B_{1g}$	13,914	1	13,790	
$^2A_{1g}$	14,200	1	14,170	$Dq = 1850$
$^2A_{2g}$	14,689	1	14,820	$Ds = 1570$
a^4E_g	17,000	1	17,010	$Dt = -50$
$^4B_{2g}$	18,500	1	18,500	$B = 790$
b^4E_g	24,300	1	24,240	$C = 2760$
$^4A_{2g}$	29,900	1	29,920	
b^2E_g	21,487	0	22,980	
$^2B_{2g}$		0	21,600	

[a] The minimum is rather flat so that values are given to ±10 cm^{-1}. [b] This value has been used to allow for the intensity of the progressions.[6]

approximations of the model and the values of the parameters are consistent with the nature of the ligands. A search was made for other plausible assignments and other least-squares minima but with negative results. If the positions of the quartets are allowed to vary by ±100 cm^{-1} to allow for experimental error, the maximum ranges of the crystal field parameters are $1862 > Dq > 1839$, $1626 > Ds > 1511$, $-23 > Dt > -85$ cm^{-1}. The calculated separation of the $^2B_{1g}$ and $^2A_{2g}$ states is larger than the observed value; a similar result has been observed previously.[6] The energy of the b^2E_g state was not fitted since it is not possible for a strong-field calculation accurately to reproduce the energies of states which correlate with more than two free ion states and indeed it is clear that, if our assignment of the b^2E_g state is correct, the calculation considerably overestimates its energy. The values of B and C cannot usefully be compared with values derived from other compounds.

The eigenvectors of the doublet states are of interest in that they should show the mixing of the cubic strong-field states that has been used to explain the changes in bond length and force constants. The contributions to the lowest doublet states that are greater than 0.1 the crystal field parameters in Table IV are

$$a^2E_g = 0.88[^2T_1(t_2^3)] - 0.44[^2T_2(t_2^3)] - 0.10[^3T_2(t_2^2(^1T_2)e)]$$

$$b^2E_g = 0.78[^2T_2(t_2^3) + 0.42[^2T_1(t_2^3) + 0.33[^2T_2(t_2^2(^1T_2)e)] - 0.21[^2T_2(t_2^2(^3T_1)e)] + 0.16[^2T_1(t_2^2(^1T_2)e)] - 0.13[^2T_2(t_2e^2(^1A_1))]$$

$$^2B_{1g} = 0.98[^2E(t_2^3)] + 0.18[^2E(t_2^2(^1A_1)e)] + 0.12[^2E(t_2^2(^1E)e)]$$

$$^2A_{1g} = 0.99[^2E(t_2^3)] + 0.15[^2E(t_2^2(^1A_1)e)]$$

$$^2A_{2g} = 0.99[^2T_1(t_2^3)] + 0.11[^2T_1(t_2^2(^1T_2)e)]$$

$$^2B_{2g} = 0.94[^2T_2(t_2^3)] + 0.22[^2T_2(t_2^2(^1T_2)e)] - 0.21[^2T_2(t_2^2(^3T_1)e)] - 0.16[^2T_2(te^2(^1A_1))]$$

where the wave functions have been tabulated by Perumareddi and the g's have been omitted for brevity. The wave functions for the a^2E_g and b^2E_g states show the extensive mixing of the $^2T_1(t_2^3)$ and $^2T_2(t_2^3)$ states previously discussed. The corresponding functions expressed in terms of the strong-field configurations are

$$a^2E_g = 0.93(xy)^2(zx) - 0.31(yz)^2(zx) + 0.17(t_2^2e \text{ configurations})$$

$$b^2E_g = 0.85(yz)^2(zx) + 0.25(xy)^2(zx) + 0.42(t_2^2e \text{ configurations})$$

These demonstrate the extent of the concentration of π-electron density in the xy plane in the a^2E_g state and the concentration of π-electron density around the z axis in the b^2E_g state. The strong-field calculations overestimate the separation of the a- and b^2E_g states and hence slightly underestimate the extent of these concentrations. The wave functions also show the considerable contribution to the b^2E_g state from t_2^2e configurations which reduces the concentration of electron density around the z axis and partly explains the lower intensity of the α_{1g}(Cr–F) progressions in the b^2E_g state compared with the a^2E_g state. The $^2B_{2g}$ state also has a significant contribution from the t_2^2e configurations which makes the assignment of the 21,487-cm^{-1} transition from the observed vibrational intervals uncertain.

Intensity of the $^4B_{1g} \rightarrow {}^2A_{2g}$ Transition. The $^4A_{2g} \rightarrow {}^2E_g(O_h)$ transition of cubic chromium(III) compounds is several times more intense than the $^4A_{2g} \rightarrow {}^2T_{1g}(O_h)$ transition. This is readily explicable since, for $10Dq = ca.$ 20,000 cm^{-1}, both transitions derive most of their intensity from the $^4A_{2g} \rightarrow {}^4T_{2g}$ transition and

$$(\langle ^4T_{2g}|H_{so}|^2E_g\rangle\langle ^4T_{2g}|H_{so}|^2T_{1g}\rangle)^2 = 2.67$$

The wave functions for the $^2B_{1g}$, $^2A_{1g}$, and $^2A_{2g}$ states in $Cr(py)_4F_2^+$ are almost the same as in the cubic compounds so that the high intensity of the $^4B_{1g} \rightarrow {}^2A_{2g}$ transition is unexpected. However the lowest ^4E_g state has a significant contribution from the $^4T_{1g}(t^2e)$ state

$$a^4E_g = 0.93[^4T_2] + 0.36[^4T_1(t^2e)] + 0.07[^4T_1(te^2)]$$

because

$$\langle ^4E_g, {}^4T_{2g}|V_{tet}|^4E_g, {}^4T_{1g}\rangle = -3^{1/2}(4Ds + 5Dt)/4 = ca.\ 2500\ cm^{-1}$$

Now $\langle ^4T_{1g}|H_{so}|^2E_g\rangle = 0$ and $\langle ^4T_{1g}|H_{so}|^2T_{1g}\rangle = 3(2i)^{1/2}\xi$ so that as $(4Ds + 5Dt)$ increases, the intensity of the $^4B_{1g} \rightarrow {}^2A_{2g}$ transition increases relative to the $^4B_{1g} \rightarrow {}^2B_{1g}$, $^2A_{1g}$ transitions. A perturbation calculation using the quadrate wave functions and the spin–orbit wave functions gives comparable intensity to the $^4B_{1g} \rightarrow {}^2A_{2g}$ and $^4B_{1g} \rightarrow {}^2B_{1g}$, $^2A_{1g}$ transitions but fails to reproduce the intensity reversal. A more thorough investigation of this phenomenon must await a full spin–orbit coupling–tetragonal field calculation.

π Bonding. Most of the features of interest in the electronic spectra of this compound are caused by the asymmetry of the second-order component of the crystal field. The fourth-order component has almost cubic symmetry. This difference in the Cp and Dq asymmetries results from the different σ and π effects of the two ligands.

The values of the McClure parameters are $\delta\sigma = 2350$ cm^{-1} and $\delta\pi = 2600$ cm^{-1}. The corresponding values for *trans*-$Cr(en)_2F_2^+$ are $\delta\sigma = 600$ cm^{-1} and $\delta\pi = 2150$ cm^{-1}; the much larger $\delta\sigma$ value for the pyridine complex is consistent with the lower basicity of pyridine compared with ethylenediamine. The larger $\delta\pi$ suggests that the pyridine acts as a significant π acceptor in this compound although the difference in $\delta\pi$ values may be due, in part, to the metal–fluorine distance being less in the pyridine compound than in the ethylenediamine. (The calculated values of $Dq(z)$ are 1770 and 1510 cm^{-1}, respectively).

Further evidence for metal–pyridine π bonding comes from the high intensity of some of the vibronic origins involving internal pyridine motions. Vibronic origins acquire intensity because of the mixing of states of odd parity into the initial and terminal crystal field states by the nuclear motion. If a vibronic origin which involves chiefly internal pyridine motion has appreciable intensity, this must indicate that there is chromium d-electron density in the pyridine ring, *i.e.*, that the pyridine acts as a π acceptor. Mixing of internal pyridine and skeletal vibrations is not sufficient to account for the high intensity of these vibronic origins.

A third source of evidence for π bonding comes from the bond length and vibrational frequency changes in the doublet states. The differences between these doublet states are caused by a redistribution of electron density among the (xy), (xz), and (yz) orbitals which are σ nonbonding. The change in Cr–F stretching frequency between the $^4B_{1g}$ and a^2E_g states reflects the strong π antibonding effect of the fluoride ligands. There is a *ca.* 13% change in the Cr–F force constant and a *ca.* 5% change in the Cr–F bond length. The force constant is therefore a less strong function of bond length than in NO.[20] This presumably reflects the ionic nature of the Cr–F bond. There is no significant change in the Cr–N distance or force constant between the a^2E_g and $^4B_{1g}$ states in the pyridine compound although there is a change in bond length in *trans*-$Cr(en)_2F_2^+$. The ϵ_u(Cr–N) stretching frequency is significantly greater in the a^2E_g state than in the $^4B_{1g}$ state. There must be a mechanism which increases the Cr–N bond strength as the electron density in the (xy) orbital is increased in *trans*-$Cr(py)_4F_2^+$ but which is inoperative in the ethylenediamine compound. This mechanism is the delocalization of the xy electron density into the pyridine rings. An analogous effect has been observed in the vibrational spectra of a series of hexacyanide complexes.

Acknowledgment. We thank the SRC for grants toward the construction of the luminescence apparatus, the PCMU service for low-energy infrared spectra, and the University of London Intercollegiate Raman Spectroscopy service. A.P.M. thanks the SRC for the award of a research studentship.

Registry No. *trans*-$[Cr(py)_4F_2]NO_3$, 27731-44-8.

References and Notes

(1) To whom correspondence should be addressed.
(2) C. D. Flint, *Chem. Phys. Lett.*, **11**, 27 (1971).
(3) J. Ferguson, H. J. Guggenheim, and D. L. Wood, *J. Chem. Phys.*, **54**, 504 (1971).
(4) C. D. Flint and P. Greenough, *J. Chem. Soc., Faraday Trans. 2*, **70**, 815 (1974).
(5) Symmetry labels are those appropriate in D_{4h} symmetry except where otherwise is indicated or obvious from context.
(6) C. D. Flint and A. P. Matthews, *J. Chem. Soc., Faraday Trans. 2*, **70**, 1307 (1974).
(7) We use the sign convention of Liehr: J. R. Perumareddi, *J. Phys. Chem.*, **71**, 3144 (1967). Other workers have used the sign convention of Ballhausen: *e.g.*, Gerlock and Slade, "Ligand-Field Parameters," Cambridge University Press, Cambridge, U.K., 1973.
(8) This argument is not restricted to D_{4h} compounds but is true for any chromophore with a holohedrized symmetry of D_{4h}.
(9) D. S. McClure in "Advances in the Chemistry of Coordination Compounds," S. Kirschner, Ed., Macmillan, New York N.Y., 1961.
(10) J. Glerup, J. Josephsen, K. Mickelsen, E. Pedersen, and C. E. Schaffer, *Acta Chem. Scand.*, **24**, 247 (1970).
(11) C. D. Flint, *J. Sci. Instrum.*, **4**, 1064 (1971).
(12) L. Dubicki, M. Hitchman, and P. Day, *Inorg. Chem.*, **9**, 188 (1970).
(13) E. Pedersen and H. Toftlund, *Inorg. Chem.*, **13**, 1603 (1974).
(14) S. S. Mitra in "Optical Properties of Solids," S. S. Mitra and S. Nudelman, Ed., Plenum Press, New York, N.Y., 1969, Chapter 14.
(15) C. J. Ballhausen in "Spectroscopy in Inorganic Chemistry," Vol. 1, C. N. R. Rao and J. R. Ferraro, Ed., Academic Press, New York, N.Y., 1970. The Duschinsky effect (C. J. Ballhausen and Aa. E. Hansen, *Annu. Rev. Phys. Chem.*, **23**, 15 (1972)) has been neglected.
(16) R. Dingle, *Acta Chem. Scand.*, **22**, 219 (1968).
(17) O. S. Mortensen, *J. Chem. Phys.*, **47**, 4215 (1967).
(18) M. D. Sturge, H. J. Guggenheim, and M. H. L. Pryce, *Phys. Rev. B*, **2**, 2459 (1970).
(19) J. A. Ladd and W. J. Orville-Thomas, *Spectrochim. Acta*, **22**, 919 (1966).

Contribution from the Department of Chemistry, University of Maryland, College Park, Maryland 20742

X-Ray Photoelectron Spectroscopy of Inorganic and Organometallic Compounds of Molybdenum[1]

SAMUEL O. GRIM* and LUIS J. MATIENZO

Received June 14, 1974 AIC40384G

X-Ray photoelectron spectra (XPS) of the Mo($3d_{3/2}$) and Mo($3d_{5/2}$) levels for about 50 compounds containing molybdenum in various oxidation states have been studied. A plot of metal binding energy *vs.* calculated charge indicates that a binding energy shift of 1 eV corresponds to a 0.3+ charge unit on molybdenum. The study of several organometallic compounds shows that strong σ-donor ligands increase the electronic density about the metal producing even lower metal binding energies than those obtained for argon-sputtered metal foil. The P(2p) binding energies of coordinated and uncoordinated phosphorus ligands are more or less constant.

Introduction

To date, only scattered X-ray photoelectron spectroscopy (XPS) data have been available on the molybdenum system.[2] Three reports in the literature have treated this problem very briefly. Swartz and Hercules[2b] have examined some fairly common molybdenum compounds (mainly molybdates) and have pointed out the application of XPS as an analytical technique for the determination of MoO_2–MoO_3 mixtures. Miller, *et al.*,[3] have used XPS to study MoO_3 catalysts supported on alumina and have been able to detect interactions between the catalyst and the support upon calcination. Clark, *et al.*,[4] have obtained data for some complexes of the type η^5-$C_5H_5Mo(CO)_2NCR_2$ and η^5-$C_5H_5Mo(CO)_2R_2CNCR_2$ and used them in conjunction with other spectroscopic data to discuss structure and bonding in these complexes. No systematic study on organometallic compounds of molybdenum, however, has yet been reported.[5] Results of investigations by Tolman, *et al.*,[6] on organometallic compounds of nickel indicate that possible oxidation or decomposition and difficulties with energy calibration demand careful interpretation of data obtained on very air-sensitive samples. A few other studies have obtained information on organometallic compounds of similar composition. Clark and Adams[7] have reported the study of chromium, iron, and nickel carbonyls and their π-cyclopentadienyls. Bis- and mono(arene)chromium carbonyls have been described recently,[8] and a short study on the charge localization of ionic derivatives of alkylferrocenes is also available.[9]

Results obtained from about 50 inorganic and organometallic compounds are presented. This study attempts to show the applicability of XPS to inorganic and organometallic compounds of molybdenum, particularly those containing phosphorus ligands, by combining newly obtained data with information provided by previous studies.

Experimental Section

The compounds used in this study were prepared, purified, and characterized according to published methods.[10-30] Air-sensitive compounds were handled under nitrogen and stored in Schlenk tubes. The compounds for which no preparative methods are given were reagent grade chemicals, used without further purification. The spectra were obtained from powdered samples mounted on cellophane tape using a Varian Associates IEE-15 electron spectrometer. The binding energy of molybdenum metal was obtained by argon sputtering